Journal of the Ceramic Society of Japan 117 [3] 245-248 2009 Paper

Synthesis of hematite particles with various shapes by a simple hydrothermal reaction

Qiang DONG,[*] Dan WANG, Jianxi YAO, Nobuhiro KUMADA,[*,†] Nobukazu KINOMURA,[*] Takahiro TAKEI,[*] Yoshinori YONESAKI[*] and Qiang CAI[**]

State Key Laboratory of Multi-Phase & Complex Systems, Institute of Process Engineering, Chinese Academy of Sciences, Beijing 100080, China

[*]Department of Research Interdisciplinary Graduate School of Medicine and Engineering, University of Yamanashi, 7, Miyamae, Kofu 400−8511

[**]Department of Materials Science and Engineering, TsingHua University, Beijing, 100084, China

Hematite particles with various shapes have been synthesized through a simple hydrothermal reaction. The particle shape and size can be controlled by adjusting pH value in the starting solution. The products were characterized by X-ray powder diffraction patterns (XRD), scanning electron microscope (SEM), transmission electron microscope (TEM), high resolution transmission electron microscope (HRTEM), FT–IR, TG–DTA and mass spectrometry of gas species during TG–DTA. The TEM and HRTEM results revealed that large numbers of micropores ranging from 0.5–0.6 nm existed in the surface of spherical particles.

Key-words : Hematite particles, A simple hydrothermal reaction, Shape and size, PH value, Spherical particles

[Received June 10, 2008; Accepted October 16, 2008]

1. Introduction

The synthesis of iron oxides has received great attention because of their potential applications in the fields of magnetic resonance imaging, catalysis and gas-sensor devices etc. Various shapes of iron oxides have been obtained by sol–gel processes, chemical oxidation in polymer or mineral matrixes, electrochemical synthesis route etc.[1)–4)] In these synthesis methods shape of the products is dependent on synthesis parameters such as concentration of the reactants, temperature and medium etc, moreover, multiple reaction steps are required to obtain the final products. While the hydrothermal precipitation method has some advantages such as fast reaction time, effective control of particle shape, and low incorporation of impurities into the particles,[5)–7)] when compared with the other preparative methods. Hydrothermal preparation is a very promising method to control morphology of the products. To our knowledge, many studies have been done on the preparation of hematite (α-Fe_2O_3), which belongs to hexagonal crystal system, by the hydrothermal reaction without additives[8)] or with organic additives such as surfactants[7),9)] and citrate.[10)] For instance, Kandori and Ishikawa[8)] have successfully prepared cubic particles with uniform micropores 0.8 nm in diameter by using $FeCl_3$ aqueous solution. Dehong Chen et al.[7)] have prepared hollow-structured hematite (α-Fe_2O_3) particles from a $FeCl_3{\cdot}6H_2O$ and NaOH solution in the presence of DBS (dodecyl benzenesulfonic acid, sodium salt). Using $(NH_4)_3Fe(C_2O_4)_3$ and NaOH as starting materials, Jing and Wu[9)] have synthesized monodispersed ellipsoidal and spherical shapes hematite (α-Fe_2O_3) nanoparticle modified by SDS (sodium dodecylsulfonate) and HPC (hexadecylpyridinium chloride), respectively. Diamandescu and Tarabasanu[10)] have synthesized acicular polycrystalline hematite (α-Fe_2O_3) particles by using $FeCl_3{\cdot}6H_2O$ and citrate. In this work, a simple hydrothermal method was successfully employed to synthesize hematite (α-Fe_2O_3) particle with different shapes and sizes from a solution of $Fe(NO_3)_3{\cdot}9H_2O$ and NaOH only by controlling the starting pH value of the solution.

2. Experimental

2.1 Synthesis of hematite particles

The concentration of NaOH solution was varied in the range of 0.1–4.0 mol dm^{-3}, while that of $Fe(NO_3)_3{\cdot}9H_2O$ solution was constant (1.00 mol dm^{-3}). $Fe(NO_3)_3{\cdot}9H_2O$ solution (8 ml) was added to NaOH solution (8 ml) at room temperature under vigorous stirring for 15 min to form $Fe(OH)_x^{+(3-x)}$ sol. Then, the sol was poured into a Teflon-lined autoclave and heated at 140°C. The reaction duration was varied from 0.5 to 12 h. The products were collected by centrifugation and washed with deionized distilled water and ethanol two times, respectively. The samples were dried in air at 50°C for 20 h.

2.2 Characterization

X-ray powder diffraction patterns (XRD) were obtained using Cu Kα radiation. Diffraction patterns were recorded from 10° to 60° with a step of 0.03°, and a scanning rate of 10 s per step. The morphologies of the particles were observed by scanning electron microscope (SEM JSM–35CF), transmission electron microscope (TEM) techniques and high resolution transmission electron microscope (HRTEM) were conducted (HRTEM JEM–2010F) with an acceleration of 200 kV to ascertain the internal structure of the final products. FT–IR spectra were recorded in the range of 4000–400 cm^{-1} on a JASCO FT/IR–4100 spectrometer, using transparent KBr pellets. TG–DTA

† Corresponding author: N. Kumada; E-mail: kumada@yamanashi.ac.jp

and mass spectrometry of gas species during TG–DTA were carried out in a Rigaku Thermo Plus TG 8120 thermal analysis system with a heating rate of 10°C min^{-1} from room temperature to 800°C under a flow of helium. The Brunauer-Emmett-Teller (BET) surface area and the porosity of spherical hematite particles were investigated by Autosorb–1 Surface Area and Pore Size Analyzer with N_2 gas adsorption measurement after evacuating the samples at 150°C.

3. Results and discussion

Figure 1 shows the X-ray patterns of the samples prepared at 140°C for 12 h at different pH values, 3, 7 and 11. All of the patterns exhibit the characteristic XRD pattern of hematite (JCPDS 33–664). The intensity of the diffraction peaks increased with pH value. It is also apparent that the width at half-maximum of the diffraction peaks decreased slightly with increasing pH value. From these results, the crystallinity and particle size of the products increased with pH value, and the proportion of the precursory complexes responsible for the precipitation of hematite is likely to increase with pH value. In the other words, higher pH value enhances the nucleation as well as the growth of the hematite.[11] **Figure 2** shows the SEM images of the samples. Spherical, diamond-like, plate-like hematite particles can be obtained as pH values are 3, 7 and 11, respectively. The corresponding particle sizes are about 100, 150 and 600 nm respectively. This trend is consistent with the result from XRD. The morphology

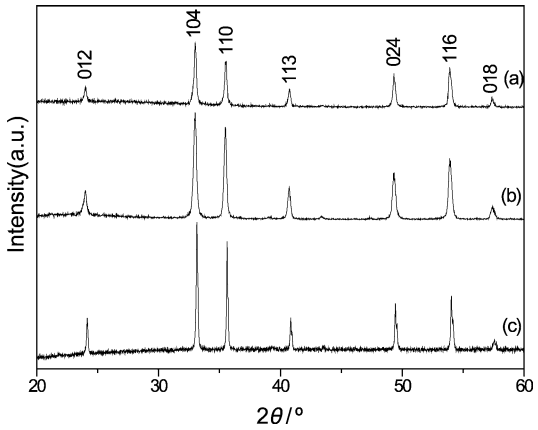

Fig. 1. XRD patterns of hematite prepared at 140°C for 12 h with different pH values (a) pH = 3, (b) pH = 7, (c) pH = 11.

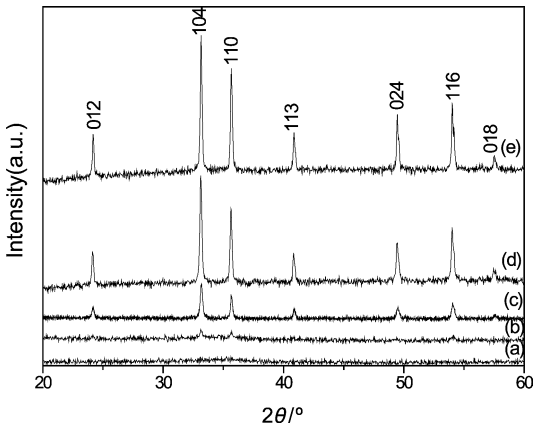

Fig. 3. X-ray powder diffraction patterns of hematite particles produced at pH = 3 with various reaction time (a) 0.5 h, (b) 1 h, (c) 1.5 h, (d) 3 h, (e) 12 h.

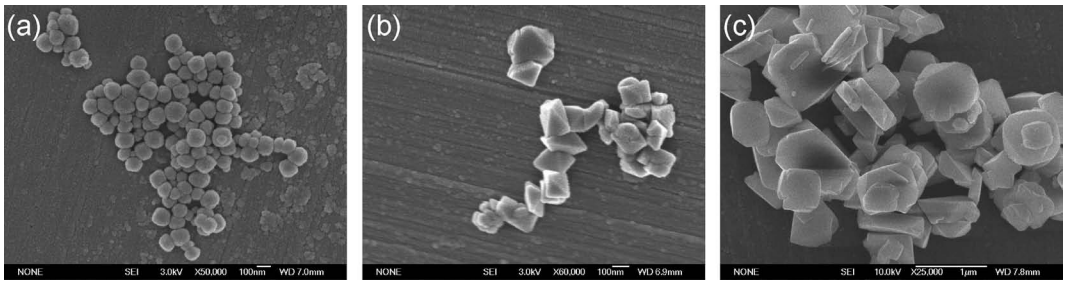

Fig. 2. SEM images of hematite particles prepared at 140°C for 12 h with different pH values (a) pH = 3, (b) pH = 7, (c) pH = 11.

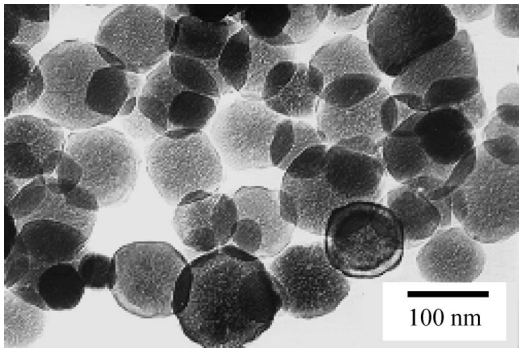

Fig. 4. TEM images of spherical hematite particles prepared at 140°C for 12 h.

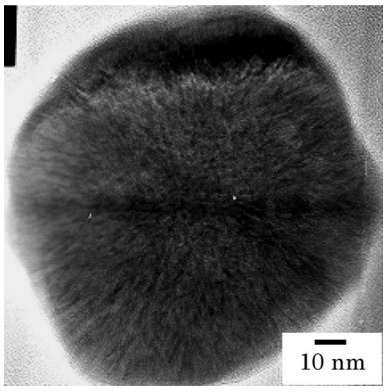

Fig. 5. HRTEM image of spherical the single particle prepared at 140°C for 12 h.

of hematite particles changes together with the particle size; small particle has spherical form, medium particle is diamond-like, and large particle is plate-like. **Figure 3** shows the X-ray powder diffraction patterns of hematite particles produced at pH = 3 with various reaction time at 140°C. The products are amorphous when reaction time is 0.5 h. After prolonging the reaction time to 1 h, the 104, 110, and 116 diffraction peaks are observed. Crystallinity of the products depends on the reaction time until 3 h and the hematite particles have crystallized when reaction time is more than 3 h.

The spherical particles were characterized by TEM observation. As shown in **Fig. 4**, the surface of the spherical hematite particles is not smooth. The roughness of the surface is considered to be caused by micropores as shown in the HRTEM image (**Fig. 5**). The size of micropores is estimated to about 0.5 nm. As shown in **Fig. 6**, the space of lattice planes is 0.36 ± 0.01 nm, it is in agreement with the literature value of the unit cell dimension of hematite, which indicates that spherical particle is a structurally uniform hematite single crystal, and is free from defects and dislocations. On the other hand, the surfaces of diamond-like and plate-like hematite particles are smooth and micropores could not be observed. N_2 gas adsorption measurement for the spherical nanoparticle was carried out in order to get information on the porosity. **Figure 7** shows the gas adsorption isotherm of hematite spherical particle. And Brunauer–Emmett–Teller (BET) surface area was calculated to be 22.45 m^2/g from the adsorption isotherm. Pore size distribution which was analyzed using Horvath–Kawazoe (HK) methods, shows that these spherical-like nanoparticles have pores with diameters of ca.0.55 nm as shown in **Fig. 8**. The measured pore diameter is in good agreement with the value observed by TEM.

Figure 9 shows the FT–IR spectra of the samples prepared at 140°C for 12 h, with different pH values, 3, 7 and 11. It can be seen that the IR spectra present similar trends. The two strong adsorption bands at about 560 and 474 cm^{-1} can be attributed to the characteristic lattice vibrations of the hematite phase.[7] Vibration bands at 1380 cm^{-1}, identified in Fig. 9(a) and (b), correspond to adsorbed NO_3^- on the particle surface. The amount of NO_3^- adsorbed on the surface of particles decreased with the increasing of pH value of the solution. The peak at 2357 cm^{-1} indicates C–O vibration of adsorbed CO_2 on the particle surfaces. Besides the adsorption peaks mentioned above, there is a broad band centered at 3430 cm^{-1} and a medium peak at ca.1650 cm^{-1} in all samples, which might be ascribed to vibration of OH groups and bending vibration of water molecules, respectively.[12] The dominant absorption peak at 570 cm^{-1} shifts to somewhat lower frequencies and becomes sharper from Fig. 9(a)–(c) when the mean crystallite diameter decreases. It is probably due to the changes of the morphology and the internal structure of the particles.[12),13)]

Figure 10 shows TG curve and gas evolution during TG measurement of spherical hematite particles measured in helium

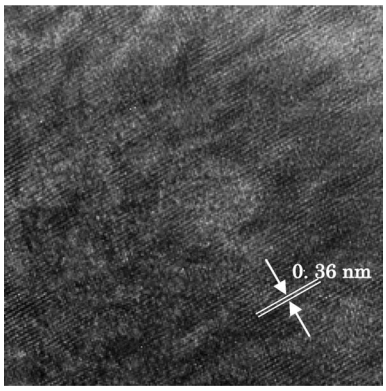

Fig. 6. Magnified HRTEM image of the spherical particle prepared at 140°C for 12 h as shown in Fig. 5.

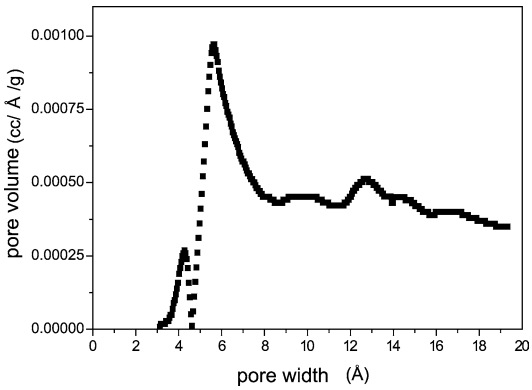

Fig. 8. Pore size distribution of spherical hematite particles prepared at 140°C for 12 h.

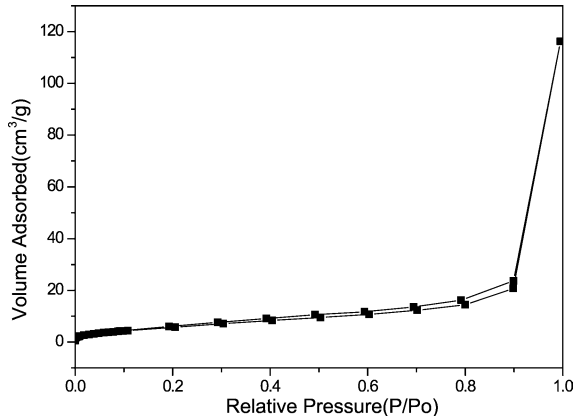

Fig. 7. N_2 gas adsorption isotherm of spherical hematite particles prepared at 140°C for 12 h.

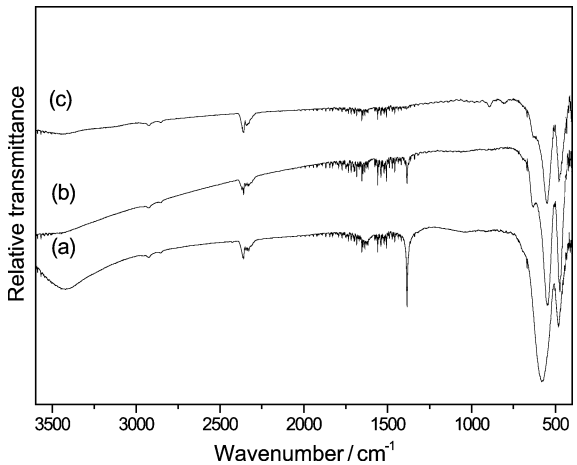

Fig. 9. IR spectra of hematite particles prepared at 140°C for 12 h with different pH values (a) pH = 3, (b) pH = 7, (c) pH = 11.

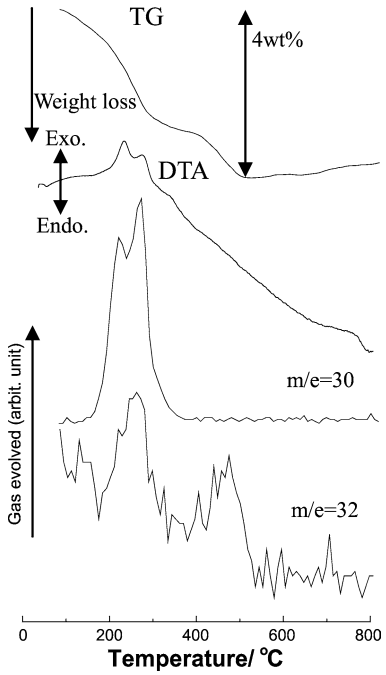

Fig. 10. TG curve and gas evolution during TG measurement of spherical hematite particles.

atmosphere at a heating rate of 10°C min^{-1}. The TG curve presents the thermal decomposition with 4% weight loss in the range of 120–471°C as shown Fig. 10, accompanied by endothermal effects. Since the spherical hematite particles adsorbed NO_3^- as shown in FT–IR spectra (Fig. 9), the m/e values, 30 and 32 in the TG-mass were assigned to NO and O_2, respectively. This weight loss at around 260°C was caused by the thermal decomposition of NO_3^- adsorbed on the surface of particles.

4. Conclusions

Hematite particles with various shapes have been successfully prepared without any additives via a simple hydrothermal method using $Fe(NO_3)_3 \cdot 9H_2O$ and NaOH as starting materials. It is clarified that the starting pH value of the solution plays an important role in the shape and size of hematite particles. This hydrothermal route can be successfully used for the synthesis of hematite particles with various shapes, which are expected to be applied in the related fields, taking the advantage of being an environmentally friendly and less energy consuming procedure.

Acknowledgment This work was partly supported by the National Natural Science Foundation of China (Grant No. 20401015, 50574082 and 20606035) and the Foundation of University of Science & Technology Beijing (No. 20050214890).

References

1) Y. Chung, S. K. Lim, C. K. Kim, Y. H. Kim and C. S. Yoon, *J. Magn. Magn. Mater.*, 272–276, 1167–1168 (2004).
2) C. Pascal, J. L. Pascal and F. Favier, *Chem. Mater.*, 11, 141–147 (1999).
3) C. P. León, L. Kador and M. Zhang, *J. Raman Spectrosc.*, 35, 165–169 (2004).
4) H. Itoh and T. Sugimoto, *J. Colloid Interface Sci.*, 265, 283–295 (2003).
5) M. Wu, T. Fujiu and G. L. Messing, *J. Non-Cryst. Solids*, 121, 407–410 (1990); A. Imhof and D. J. Pine, *Nature* (London)., 389, 948–950 (1997); D. Walsh and S. Mann, *Nature*, 377, 320–322 (1995); V. N. Manoharan, A. Imhof, J. D. Thorne and D. J. Pine, *Adv. Mater.*, 13, 447–450 (2001).
6) L. Qi, J. Li and J. Ma, *Adv. Mater.*, 14, 300–305 (2002); D. Zhang, L. Qi, J. Ma and H. Cheng, *Adv. Mater.*, 14, 1499–1503 (2002); R. K. Rana, Y. Mastai and A. Gedanken, *Adv. Mater.*, 14, 1414–1418 (2002); M. Iida, T. Sasaki and M. Watanabe, *Chem. Mater.*, 10, 3780–3785 (1998).
7) D. H. Chen, X. Jiao and Y. Zhao, *J. Mater. Chem.*, 13, 2266–2270 (2003).
8) K. Kandori and T. Ishikawa, *J. Colloid Interface Sci.*, 272, 246–248 (2004).
9) Z. Jing and S. Wu, *Mater. Res. Bull.*, 39, 2057–2064 (2004).
10) L. Diamandescu and D. M. Tarabasanu, *Ceram. Inter.*, 25, 689–692 (1999).
11) J. H. Zhang, Q. H. Kong, J. Dua, D. K. Ma, G. C. Xi and Y. T. Qian, *J. Cryst. Growth.*, 308, 159–165 (2007).
12) Z. H. Jing, S. H. Wu, S. M. Zhang and W. P. Huang, *Mater. Res. Bull.*, 39, 2057–2064 (2004).
13) D. H. Chen, X. L. Jiao and D. R. Chen, *Mater. Res. Bull.*, 36, 1057–1064 (2001).